archaeometry

Archaeometry **60**, 1 (2018) 171–182 doi: 10.1111/arcm.12329

AN APPROACH TO THE DIAGNOSIS OF CRANIOFACIAL FIBROUS DYSPLASIA FROM THE 2500-YEAR-OLD REMAINS OF A SKULL FROM ANCIENT CHINA*

Z. Z. SHI,[1]‡ Q. ZHANG,[2]‡ K. L. CHENG,[3] H. SHAO,[1] D. ZHAO,[4] B. T. SUN,[1] J. YU,[5] Z. C. SUN,[2] M. C. LI,[2] L. GUO,[2] H. ZHU,[2] Q. C. ZHANG[2]† and Y. H. HUANG[4,6]†

[1]*Department of Hematology and Oncology, China–Japan Union Hospital, Jilin University, Changchun Jilin 130033, China*

[2]*Research Centre for Chinese Frontier Archaeology of Jilin University, Changchun, Jilin 130012, China*

[3]*Department of Radiology, China–Japan Union Hospital, Jilin University, Changchun, Jilin 130033, China*

[4]*Science Research Centre, China–Japan Union Hospital, Jilin University, Changchun, Jilin 130033, China*

[5]*Department of Nephrology, China–Japan Union Hospital, Jilin University, Changchun, Jilin 130033, China*

[6]*College of Life Science and Bioengineering, Beijing University of Technology, Beijing 100000, China*

A human skull, buried about 2500 years ago in a Bronze Age cemetery at Jinggouzi, a site of an important ethnic group in ancient China, appeared to have characteristics of fibrous dysplasia. The CT images indicated a reduction in bone density and relatively homogeneous lesions. More features were revealed using CT reconstruction techniques. Lesions seen in low-magnification images using a 3D deep-field microscope had an irregular honeycomb-like structure. At higher magnification, the trabeculae morphology and the gaps between the trabeculae were irregular and varied in size and shape. Paraffin-embedded specimens stained with HE showed trabeculae with tortuous irregular arrangements varying in shape and width. The irregular trabeculae of woven bone has been described as having fibrous dysplasia. Molecular analysis of the GNAS gene indicated no mutation. This provides a non-invasive approach for us to make more comprehensive diagnoses and to assist research into ancient human diseases.

KEYWORDS: COMPUTED TOMOGRAPHY (CT), PALAEOPATHOLOGY, ANCIENT DNA, FIBROUS DYSPLASIA

INTRODUCTION

The study of ancient populations across thousands of years of human history greatly helps our understanding of the pathogenesis of human diseases (Thompson *et al*. 2013). The premise of this work is the diagnosis of ancient diseases (de Boer *et al*. 2013). With progress in biology and medicine, archaeologists and palaeopathologists can obtain a great deal of biological information from ancient human specimens (Thompson *et al*. 2013). More information can be obtained from well-preserved specimens, including relatively detailed information at the level of tissue cytology and molecular biology (Mitchell *et al*. 2013; Schuenemann *et al*. 2013; Appleby *et al*. 2014). This provides the opportunity for us to make more comprehensive diagnoses to assist further research into ancient human diseases (Gerszten *et al*. 2012; Thompson *et al*. 2013; Appleby *et al*. 2014). However, since cases of rare diseases reported in the literature for ancient humans are obviously very

*Received 14 June 2016; accepted 29 April 2017

†Corresponding authors: py2000sdqy@sina.com and yhuang@bjut.edu.cn

‡The first two authors contributed equally to this paper.

limited, advanced techniques need to be employed to make more comprehensive diagnoses of ancient disease (Papagrigorakis *et al*. 2012; Monge *et al*. 2013).

Computed tomography (CT) plays an important role in exploring ancient human diseases (Wu and Schepartz 2009; Wade *et al*. 2012; Thompson *et al*. 2013). In the HORUS study, the use of CT clarified key points in the diagnosis of ancient coronary artery diseases (Thompson *et al*. 2013). This non-invasive imaging method can reveal radiographic features in blind spots and reduce any possible damage to the specimen by avoiding other more invasive endoscopic techniques (Cavka *et al*. 2012). Various CT reconstruction techniques have had a significant impact on bioarchaeology (Cavka *et al*. 2012; Wade *et al*. 2012; Thompson *et al*. 2013). However, most reports on CT reconstruction techniques, tissue transition projection (TTP) and CT virtual endoscopy (CTVE) are in the field of modern medicine and there are few reports in archaeology (Willmon *et al*. 2013). CT reconstruction techniques were used in our research to reveal the bone lesions of fibrous dysplasia (FD).

In modern medicine, the clinical features of FD include cranial asymmetry, facial deformity, hearing loss, proptosis, visual impairment and unilateral blindness when the optic foramen is involved (Lee *et al*. 2012a). Craniofacial FD is a rare disease and only a few case reports of ancient humans with the disease have been found in the literature (Wells 1963; Canalis *et al*. 1980; Gregg and Reed 1980; Papagrigorakis *et al*. 2012; Monge *et al*. 2013).

A paraffin section with a haematoxylin and eosin (HE) stain is the main means of clinicopathological diagnosis. HE staining of bone samples is used in modern medicine more widely than in archaeology (Schultz 2001; Gerszten *et al*. 2012; de Boer *et al*. 2013). Some researchers have found that dry bone samples without decalcification can improve diagnostic power (de Boer *et al*. 2012). We attempted to observe the microstructure of the lesions by HE staining. An optical depth-of-field microscope was used to view the section; such a microscope is generally used in the field of engineering, and is seldom used in palaeopathology.

Craniofacial FD is a disorder caused by a GNAS gene mutation that leads to the normal structure of bone being replaced by woven bone trabeculae and fibrous tissue (Lee *et al*. 2012a). The GNAS locus at 20q13.2–q13.3 encodes the α subunit of the Gs G-coupled protein receptor. In bone, constitutive Gsα signalling results in impaired differentiation and proliferation of bone marrow stromal cells. Proliferation of these cells causes replacement of normal bone and marrow with fibrous tissue.

The abnormal skull specimen that is the focus of this research was recovered from Jinggouzi (about 2485 BP), a Bronze Age cemetery site in the east of the ancient Great Wall region in northern China. We found that the specimen seemed to have a cranial FD lesion. This study developed an appropriate combined approach using CT technology and microscopic images to diagnose FD. We also tried to use molecular biology to help with the diagnosis.

MATERIALS AND METHODS

Sample

The skull specimen (Fig. 1) was discovered at Jinggouzi cemetery in Linxi County, Chifeng City, Inner Mongolia Autonomous Region, in northern China. It is located on the north bank of the Xar Moron River and south of the extension of the Greater Khingan Mountains. Between 2002 and 2003, with the permission of the State Administration for Cultural Heritage, 58 nomad tombs were excavated in an area of 1870 m^2 by the Research Centre for Chinese Frontier Archaeology of Jilin University. The direction of these tombs is north-west – south-east. The vast majority of

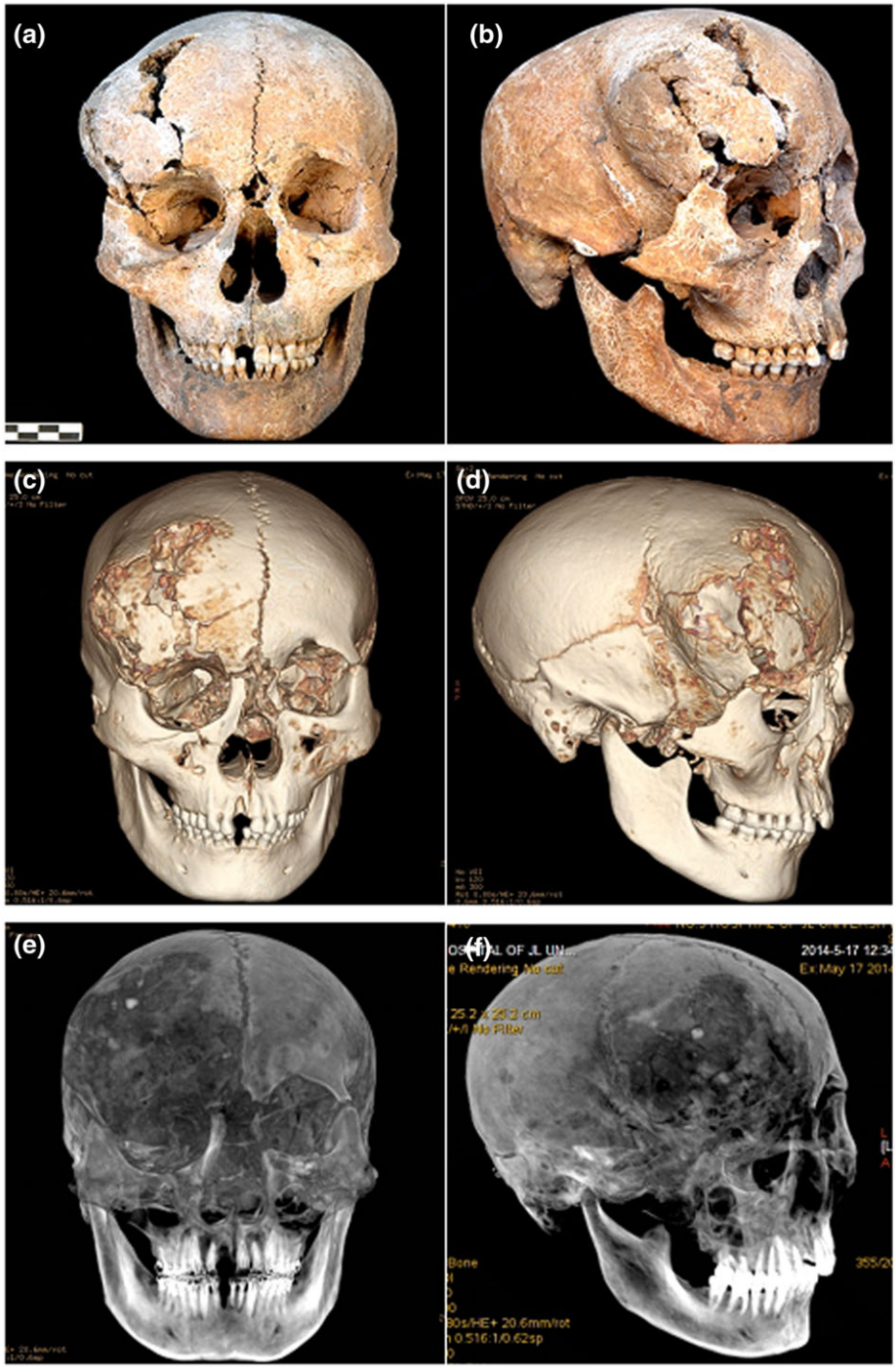

Figure 1 *Colour photographs taken with an ordinary camera (a, b), shaded surface display (SSD) images (c, d) and maximum intensity projection (MIP) images (e, f). [Colour figure can be viewed at wileyonlinelibrary.com]*

the tombs contained multiple individuals. The most prevalent burial objects consisted of bone artefacts, pottery, bronze ornaments and arrowheads made of deer antler, which represent an early nomadic population of the ancient DongHu people—a famous ancient nomadic ethnic group that has played an important role throughout Chinese history (Wang *et al*. 2010). After excavation, all the finds, including the specimen, were preserved at the Research Centre for Chinese Frontier Archaeology, Jilin University.

The specimen belonged to an individual labelled 02LJM55:B, from tomb M55, which was a nearly rounded trapezoid vertical tomb similar to other tombs (Wang *et al*. 2010). No similar abnormality as in this specimen was found among the other skulls. Five individuals in the tomb were all disturbed after burial due to a custom in this region. Both sides of the tibia and fibula of individual M55B were missing. The other individuals in this tomb were incomplete adolescents and infants. Carbon dating was conducted and provided a date of 2485 ± 45 BP. The dating result is in accordance with the archaeological cultural characteristics and falls within the Bronze Age in China (Wang *et al*. 2010). The sex and age of this individual were determined based on the skeletal remains using the pubic symphysis, the innominate bone and the cranium (Brooks and Suchey 1990; Buikstra and Ubelaker 1994). Various skeletal indicators, such as pubic symphyseal morphology, dental wear and some features on the skull, suggested that the individual was a male who died at the age of approximately 22 years old.

CT Imaging and 3D reconstruction

The skull was scanned using a 64-slice CT, GE Discovery High Definition 750 CT scanner (GE Healthcare, Milwaukee, WI, USA), using 120 kV and 300 mAs. The field of observation was 25 cm and the slice thickness of the reconstruction was 0.6 mm. CT scan data were reconstructed using the advanced volumeshare 4.0 (ADW4.0) imaging software on a CT workstation. Multiple techniques, including shaded surface display (SSD), multiplanar reconstruction (MPR), maximum intensity projection (MIP), TTP and CTVE, were employed in image analysis and secondary image reconstruction.

Histopathological observation

Some lesion tissue specimens were observed directly with a VHX-2000 series microscope (KEYENCE). Unlike conventional optical microscopes, it has a real-time zoom lens (RZlens) and a high dynamic range (HDR) function, synthesizing three-dimensional (3D) images by capturing multiple colour images at different brightness levels to observe the specimens. Other lesion tissue specimens were fixed with formalin, before being embedded in paraffin and stained with HE.

Genomic DNA extraction and amplification

The DNA extraction protocol used followed published methodologies (Ong *et al*. 1998; Rohland and Hofreiter 2007). Genomic DNA was amplified using the arbitrary primer PCR technique. Seven arbitrary primers were used, as follows: (1) 5′-CCGGCTACGG; (2) 5′-CAGGCCCTTC; (3) 5′-AACGGTCACG; (4) 5′-AGCTGCCGGG; (5) 5′-AGGCATTCCC; (6) 5′-GGTCTGAACC; and (7) 5′-AAGGCTAACG. Genomic DNA extracted from the ground power of the upper left 7th tooth from a healthy individual (Dr Y. Huang) was used as a control.

RESULTS

Visual inspection

Colour photographs (Fig. 1) taken with an ordinary camera showed bulging growth in the right frontal and orbital bone. The remains were relatively intact after the fragments had been joined together with glue, and parts of the sphenoid and occipital bones are absent. Simultaneously, the optical canal and bone surrounding the nerve could not be seen clearly with the naked eye.

Cranial asymmetry and facial deformity could be seen because of the existence of lesions. There may have been proptosis as a result of the change in shape and smaller volume of the right side of the orbit. The SSD imaging results were similar to the external gross morphology observed with the naked eye. The MIP images showed low-density lesions, visible on the right side.

Imaging and 3D reconstruction

Coronary and axial MPR images (Fig. 2) showed FD lesions in the right of the skull. Localized differential bulging of the disease involved great wings of sphenoid bone, frontal bone and temporal bone. The tissue of the lesion was discontinuous and broken into irregular fragmentation and the central structure of the lesion was absent. The bone around the region of the right optic nerve canal was defective in the MPR images (Fig. 2).

We found that the texture of the lesion area was relatively uniform, with a ground glass change and cortical hyperplasia at the edge of the involved bones in (a), (b) and (c), which were axial, sagittal and coronary MPR images, respectively. The structures of the involved bones were clear, and no fusion was found between the adjacent bones. MPR images of the right orbit showed that the lesion involved the right lateral and upper walls, with a reduction of orbital volume, and clinical presentation of exophthalmos may have occurred. A change in the orbital structure can lead to the restriction of eyeball movement, and strabismus and diplopia may present. The left optic nerve canal was complete in the axial (d), sagittal (e) and coronary (f) MPR images. The bone in the region of the right optic nerve canal was incomplete and just at the edge of a lesion in (g), (h) and (i), which were axial, sagittal and coronary MPR images, respectively. The right optic nerve could have been affected, consequently including abnormal vision.

In Figure 1, the SSD images showed that the surface of the bulge lesions was smooth except where broken. The MIP images showed low-density lesions visible on the right side. Furthermore, using TTP technology, a disturbance of the endometrial structure in the FD lesions was revealed, as shown in Figures 3 (a) and 3 (b). The morphology of the intracranial membranes and the hollow organs was displayed clearly and completely in the TTP images.

Virtual endoscopy was also applied to observe the right orbit and the internal structure of the skull. The bones of the lesion area bulged into the internal cranium and the cortical bone was incomplete. Irregular sutures had formed in the lesion (Fig. 3 (c)). The entrance to the right optic nerve canal is displayed clearly in Figure 3 (d), and the wall of the right optic nerve canal was complete, as displayed in Figure 3 (e).

Microscopic and pathological findings

Using a 3D deep-field microscope, the gross specimen of the lesion showed loose bone-like tissue. Because the disordered trabeculae were connected to each other, the lesions as seen in

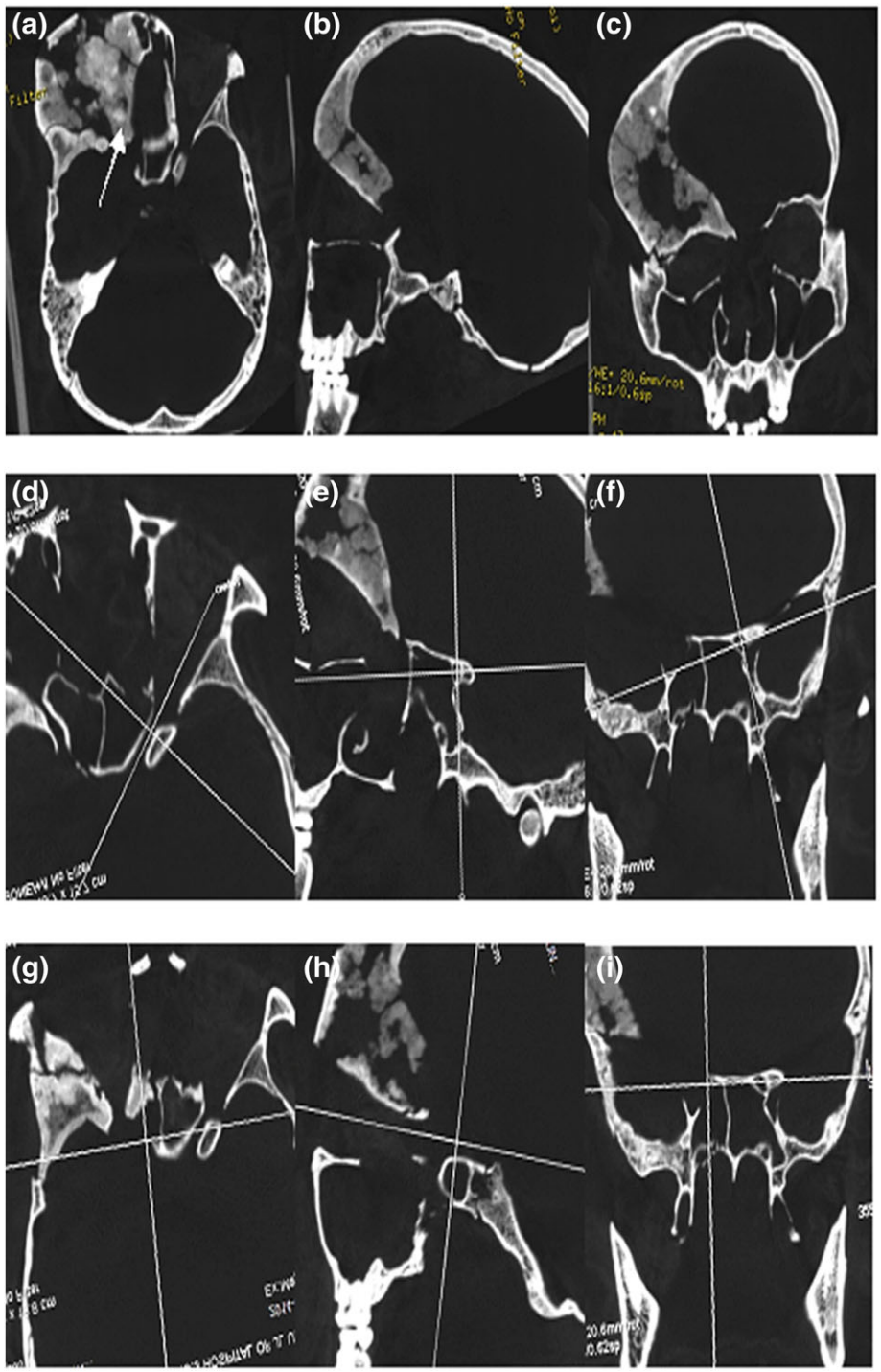

Figure 2 *Multiplanar reconstruction (MPR) images of the lesion (a–c), the left optic nerve canal (d–f) and the region of the right optic nerve canal (g–i). [Colour figure can be viewed at wileyonlinelibrary.com]*

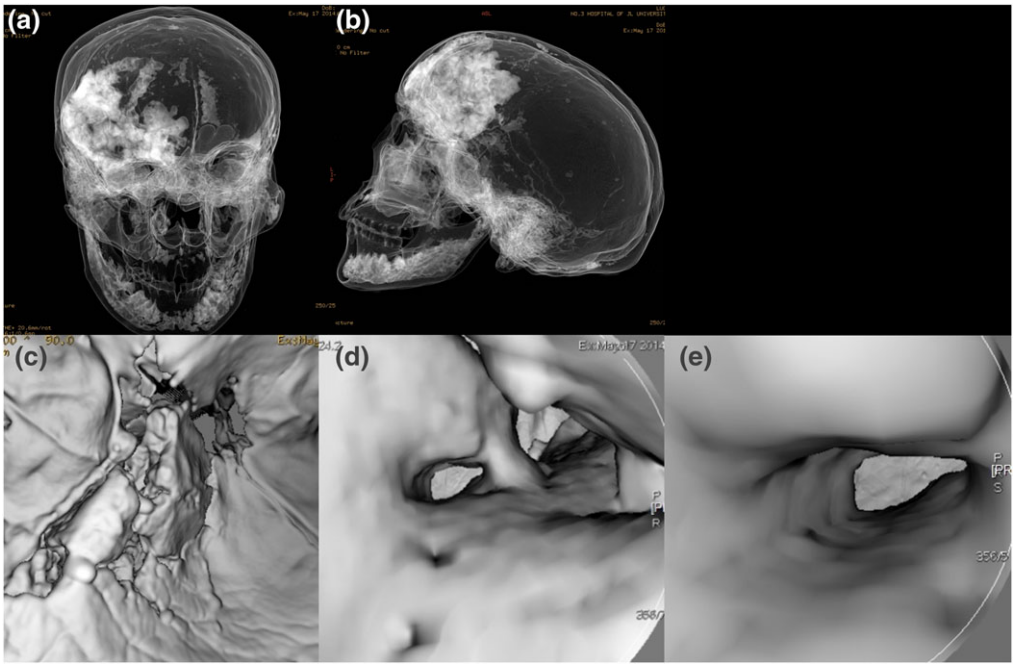

Figure 3 *Tissue transition projection (TTP) images (a, b) and CT virtual endoscopy (CTVE) (c–e): (a) the right frontal sinus was pressured and was not displayed clearly; (b) the cavity of the left frontal sinus, which shifted to the left with the sagittal suture, was shown clearly; (c) in the bones of the lesion area, irregular sutures have formed in the lesion; (d) the entrance to the right optic nerve canal; (e) the wall of the right optic nerve canal. [Colour figure can be viewed at wileyonlinelibrary.com]*

low-magnified images (Figs 4 (a) and 4 (b)) had an irregular honeycomb-like structure. At higher magnification (Fig. 4 (c)), the trabeculae morphology and the gap between the trabeculae were irregular and varied in size and shape, and part of the margin of the trabeculae showed wormhole-like changes.

By HE staining in the paraffin-embedded specimen, we found that the trabeculae with a tortuous irregular arrangement varied in shape and width (Fig. 5). The appearance of irregular trabeculae of woven bone has been described as having a Chinese-like character. The distance between trabeculae varied and the edge of the trabeculae was not smooth. The distribution between the trabeculae was uneven.

GNAS gene detection

Genomic DNA was extracted from the teeth and amplified by arbitrary primer PCR. Using arbitrary primers 2 and 4 as described in the methods section, we successfully detected the DNA. We failed to get enough DNA for subsequent gene analysis using other primers. To detect the GNAS gene, we designed a pair of primers to cover exons 8 and 9 of the GNAS gene, where the mutation on codon 201 (C → T) has been indicated in this disease. The GNAS gene exon 8 and 9 coding regions were amplified by PCR using a forward primer, 5′-CCC TCT TTC CAA ACT ACT CC-3′, and a reverse primer, 5′-AAG CCC ACA GCA TCC TAC-3′.

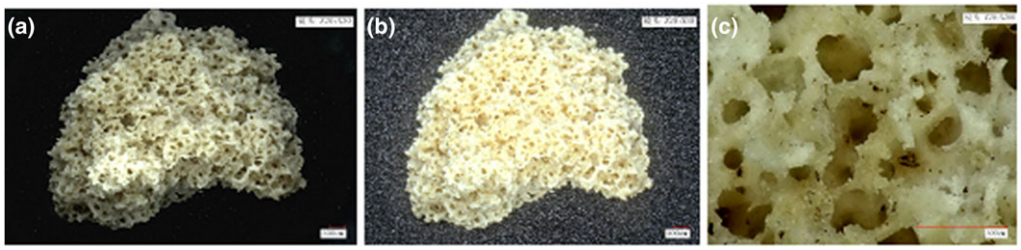

Figure 4 *Observation by the 3D deep-field microscope: (a) real-time zoom lens (RZlens) imaging (magnification ×30); (b) High dynamic range (HDR) function imaging, synthesizing 3D images by capturing multiple colour images at different brightness levels (magnification ×30); (c) RZlens imaging (magnification× 200). [Colour figure can be viewed at wileyonlinelibrary.com]*

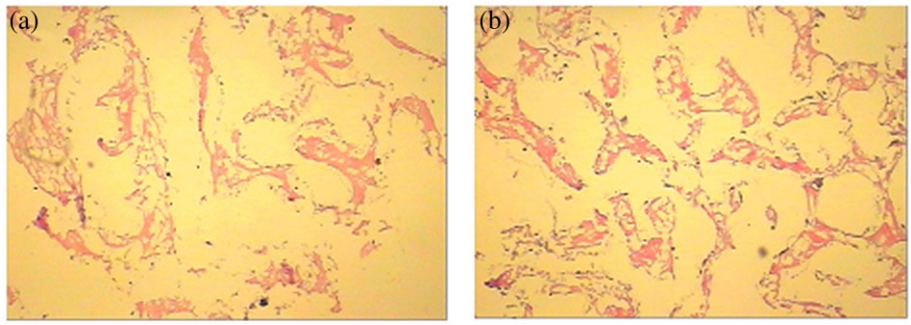

Figure 5 *Paraffin-embedded lesion samples stained with HE (magnification 10× 10). [Colour figure can be viewed at wileyonlinelibrary.com]*

We successfully obtained a positive result after amplifying the GNAS gene by PCR from the two teeth specimens of the human skull 03LJM55B, as shown in Figure 6. However, when we sequenced the amplified PCR fragment, we did not find any gene mutation. Our results suggest that, in this ancient human, FD might not have presented with a codon 201 mutation, or this specific mutation may have occurred at a later stage of evolution.

DISCUSSION

Modern medical research has provided the foundation for our study of ancient human disease (Mitchell *et al*. 2013; Schuenemann *et al*. 2013; Thompson *et al*. 2013; Appleby *et al*. 2014). Several CT reconstruction methods, such as MPR, TTP and so on, microscopic pathology techniques and molecular biology were used innovatively to diagnose the craniofacial FD. The archaeological remains of ancient humans are mostly bones and teeth—the skin and soft tissues rarely survive. Therefore, the clinical characteristics of this archaeological specimen are speculations based on morphological changes of the bone. The information provided by CT scanning is the basis of a diagnosis of FD. From a radiological point of view, the manifestations in the CT images include a reduction in bone density and relatively homogeneous lesions of the bone (Sontakke *et al*. 2011; Lee *et al*. 2012a). The findings from our study and other relevant research show that radiographic features are very similar between ancient and modern cases. The homogeneous density of the lesions is probably because the cells and stromal components in the lesion

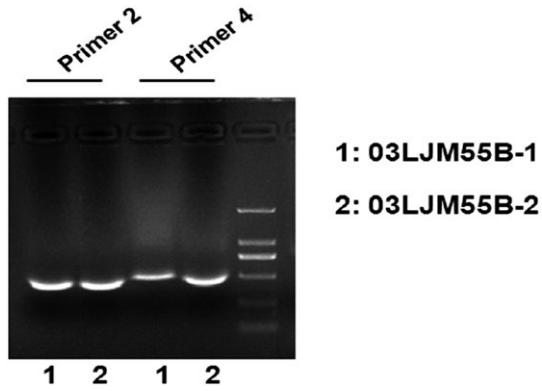

Figure 6 *GNAS gene detection: the accession number of the specimen is 03LJM55B. Two samples (1, 2) from the teeth of the specimen were analysed simultaneously by PCR. Primers 2 and 4 were used for arbitrary DNA amplification.*

have a stochastic distribution, and after about 2500 years these cells and stromal components have been reduced at random. The radiographic features and pathological results confirmed this. There was no damage to the cortical bones surrounding the lesion, except for cortical bone thickening as a result of the slow progress of the disease. This change is in accordance with the biological characteristics of FD (Papagrigorakis *et al*. 2012). Because there were no positive visual findings in other parts of the skeleton, CT scanning of other parts of the skeleton was not undertaken.

Archaeologists and physical anthropologists sometimes apply MPR and SSD when researching ancient human bone specimens (Lee *et al*. 2012a). This can help us see obvious radiographic features on the most suitable plane. MPR imaging has a direct clinical significance in determining changes in the optic canal. The location and extent of lesions can be displayed clearly from different angles using intuitive and 3D SSD images. Because the characteristics of ancient human bone specimens include the presence of a closed or partially closed cavity structure, similar to the airway and intestinal structures of modern living human bodies, we not only used conventional reconstruction techniques, but also applied TTP and CTVE to rebuild the hollow skull and research FD concurrently. TTP images, which are often used to show the bowel wall structure in clinical practice (Sontakke *et al*. 2011), provide a non-invasive evaluation of the morphology of the intracranial membranes. Tissues and organs adjacent to lesions, especially hollow organs such as the sinus cavities, are displayed clearly and completely.

Virtual endoscopy is an important screening and diagnostic tool in a clinical setting. Some researchers have yet to apply this to ancient human specimens. Virtual endoscopy can be used to observe unknown cavity structures non-invasively; for example, the complete cranial cavity and the close bone marrow cavity of long bones. Some endoscopes can provide magnified images directly. TTP and virtual endoscopy provide a potential method for future research in physical anthropology, including the identification of race and gender by means of the morphology of intracranial membranes, the comparison of femoral morphology (including bone marrow cavity characteristics) and mechanical analyses to determine aspects of human activity.

Histopathology can be used to differentiate FD from other similar diseases (Lee *et al*. 2012a; Willmon *et al*. 2013). The pathological diagnosis of FD is based primarily on changes in the trabeculae. Because the tissue and cellular components that existed between the trabeculae have disappeared, the only remains found in ancient specimens are the trabeculae themselves. We revealed some microscopic image features using 3D depth-of-field observation, including an

irregular honeycomb-like structure of a lesion and a change in the trabeculae morphology. By observing paraffin sections with HE staining, we found that the morphology of the trabeculae from the archaeological specimen was very similar to modern human sections of FD (Guinebretiere *et al*. 2013). This supports the diagnosis of FD. The random distribution of the residual trabeculae contributes to the relatively uniform density of the CT images.

Usually, FD with the involvement of one or multiple sites of bone is the result of a GNAS mutation (Lee *et al*. 2012a). The disease is called McCune–Albright syndrome, also known as Albright syndrome, if multiple systems are involved (Abdelkarim *et al*. 2008; Lee *et al*. 2012a). The detection of gene mutations contributes to the differential diagnosis in the early screening of patients with Albright syndrome (Lietman *et al*. 2005; Chapurlat and Orcel 2008; Lee *et al*. 2012b). Research on ancient DNA has been a problem because in almost all ancient specimens, DNA is only present in very tiny amounts and in various states of degradation. In our laboratory, we have succeeded in establishing DNA ultramicroanalysis techniques from cells using an improved silica method. Genomic DNA was successfully extracted from the teeth, even though the samples were from a 2500-year-old ancient human. This success was probably due to the fact that the area of the evacuation in China is very dry, and the tooth provided a rather closed environment that prevented the DNA from being degraded. We successfully obtained a positive result after amplifying the GNAS gene by PCR. Interestingly, in this case no codon 201 mutation was found by gene sequencing; therefore, our results suggest that, in ancient humans, FD might not present with this specific mutation, although the CT and microscopic images showed the pathological changes. We recognize that many neoplastic diseases involve specific changes at the genetic level, and it is generally thought that the occurrence of diseases is due to the accumulation of genetic changes. However, our study suggests that certain genetic changes could be the consequence rather than the cause of the disease, at least in FD.

FD also needs to be identified with some skeletal-related diseases. Usually, Paget's disease, osteomyelitis, meningioma and osteosarcoma can be distinguished from FD in CT imaging (Chapurlat and Orcel 2008; Unal Erzurumlu *et al*. 2015). Patients with Paget's disease are older than those with FD (Unal Erzurumlu *et al*. 2015). The appearance of osteomyelitis is diffuse sclerosis, with intermingled sclerotic and lytic lesions (Van Merkesteyn *et al*. 1988). Periosteal response is usually found in osteosarcoma (Unal Erzurumlu *et al*. 2015). Pathology can help to identify some rare bone tumours, such as low-grade intraosseous-type osteosarcoma (LGIOS), which overlap with FD imaging (Bertoni *et al*. 1993). Erosion of the endosteal cortical bone and cortical erosion have been found in most LGIOS cases (Bertoni *et al*. 1993). Immunohistochemistry may also be helpful in identifying ossifying fibroma and FD (Toyosawa *et al*. 2007). Some ossifying fibroma have similar features in CT and pathology compared to FD; therefore, detection of the GNAS mutation may be of benefit in the diagnosis of FD, or to further confirm a pathological diagnosis if the pathological results are also uncertain (Toyosawa *et al*. 2007; Chapurlat and Orcel 2008).

CONCLUSIONS

The application of modern medicine to research into ancient human tissue samples can help to achieve a relatively reliable diagnosis of ancient diseases, including some rare diseases such as FD. The non-invasive observation of ancient human specimens using CT can provide us with much more detailed morphological information about the lesions. Clinical pathology and depth-of-field optical microscopic imaging technology mean that the study of residual tissue lesions can become more accessible for researchers, providing important evidence for the diagnosis

of FD. The combination of CT and histopathology provides more comprehensive information about ancient human disease and improves the credibility of the diagnosis. As well as diagnosing ancient rare diseases by applying techniques from the fields of engineering science and modern medicine, we can also diagnose other ancient human diseases that are common in modern society, such as cancers, cardiovascular disease and trauma. The ultimate aim of our research is to view disease across human history, rather than just focusing on the today's diseases, and the results will be highly significant for an understanding of disease progression.

ACKNOWLEDGMENTS

This work is supported by the following projects: the Nation Natural Science Foundation of China (81071662), the Jilin Foundation Science and Technology (20100945, 2011756), the Major Program of the National Social Science Fund of China (Grant No. 11&ZD182), the Fok Ying Tung Education Foundation for Young Teachers (Grant No. 141111), the MOE Project of Key Research Institute of Humanities and Social Sciences at Universities (15JJD780004) and the Fundamental Research Fund of Jilin University. We are most grateful to Haotong Xu (CT suite of Physical Anthropology Institute, Kyoto University, Sakyo, Kyoto 606-8502 Japan) for his assistance in obtaining parts of 3D structures and for his contribution to the writing of the paper.

REFERENCES

Abdelkarim, A., Green, R., Startzell, J., and Preece, J., 2008, Craniofacial polyostotic fibrous dysplasia: a case report and review of the literature, *Oral Surgery, Oral Medicine, Oral Pathology, Oral Radiology*, **106**(1), e49–e55.

Appleby, J., Mitchell, P. D., Robinson, C., Brough, A., Rutty, G., Harris, R. A., Thompson, D., and Morgan, B., 2014, The scoliosis of Richard III, last Plantagenet King of England: diagnosis and clinical significance, *Lancet*, **383**(9932), 1944.

Bertoni, F., Bacchini, P., Fabbri, N., Mercuri, M., Picci, P., Ruggieri, P., and Campanacci, M., 1993, Osteosarcoma: low-grade intraosseous-type osteosarcoma, histologically resembling parosteal osteosarcoma, fibrous dysplasia, and desmoplastic fibroma, *Cancer*, **71**(2), 338–45.

Brooks, S., and Suchey, J. M., 1990, Skeletal age determination based on the os pubis: a comparison of the Acsádi–Nemeskéri and Suchey–Brooks methods, *Human Evolution*, **5**(3), 22738.

Buikstra, J. E., and Ubelaker, D. H., 1994, Standards for data collection from human skeletal remains, Report Number 44, Arkansas Archaeological Survey, Fayetteville, AR.

Canalis, R. F., Aragon, R. M., Cabieses, F., and Hanafee, W. N., 1980, Fibrous dysplasia: findings in a pre-Columbian skull, *American Journal of Otolaryngology*, **1**(2), 131–5.

Cavka, M., Petaros, A., Boscic, D., Kavur, L., Jankovic, I., Despot, R., Trajkovic, J., and Brkljacic, B., 2012, Scenes from the past: CT-guided endoscopic recovery of a foreign object from the cranial cavity of an ancient Egyptian mummy, *Radiographics*, **32**(7), 2151–7.

Chapurlat, R. D., and Orcel, P., 2008, Fibrous dysplasia of bone and McCune–Albright syndrome, *Best Practice & Research: Clinical Rheumatology*, **22**(1), 55–69.

de Boer, H. H., Aarents, M. J., and Maat, G. J. R., 2012, Staining ground sections of natural dry bone tissue for microscopy, *International Journal of Osteoarchaeology*, **22**(4), 379–86.

de Boer, H. H., Van der Merwe, A. E., and Maat, G. J. R., 2013, The diagnostic value of microscopy in dry bone palaeopathology: a review, *International Journal of Paleopathology*, **3**(2), 113–21.

Gerszten, E., Allison, M. J., and Maguire, B., 2012, Paleopathology in South American mummies: a review and new findings, *Pathobiology*, **79**(5), 247–56.

Gregg, J. B., and Reed, A., 1980, Monostotic fibrous dysplasia in the temporal bone: a late prehistoric occurrence, *American Journal of Physical Anthropology*, **52**(4), 587–93.

Guinebretiere, J. M., Kreshak, J., Suciu, V., Maulmont, C. D., Mascard, E., Missenard, G., Larousserie, F., and Vanel, D., 2013, How to read a pathology report of a bone tumor, *European Journal of Radiology*, **82**(12), 2092–9.

Lee, J. S., FitzGibbon, E. J., Chen, Y. R., Kim, H. J., Lustig, L. R., Akintoye, S. O., Collins, M. T., and Kaban, L. B., 2012a, Clinical guidelines for the management of craniofacial fibrous dysplasia, *Orphanet Journal of Rare Diseases*, **7**(Suppl. 1), S2.

Lee, S. E., Lee, E. H., Park, H., Sung, J. Y., Lee, H. W., Kang, S. Y., Seo, S., Kim, B. H., Lee, H., Seo, A. N., Ahn, G., and Choi, Y. L., 2012b, The diagnostic utility of the GNAS mutation in patients with fibrous dysplasia: meta-analysis of 168 sporadic cases, *Human Pathology*, **43**(8), 1234–42.

Lietman, S. A., Ding, C., and Levine, M. A., 2005, A highly sensitive polymerase chain reaction method detects activating mutations of the GNAS gene in peripheral blood cells in McCune–Albright syndrome or isolated fibrous dysplasia, *Journal of Bone & Joint Surgery*, **87**(11), 2489–94.

Mitchell, P. D., Yeh, H. Y., Appleby, J., and Buckley, R., 2013, The intestinal parasites of King Richard III, *Lancet*, **382**(9895), 888.

Monge, J., Kricun, M., Radovcic, J., Radovcic, D., Mann, A., and Frayer, D. W., 2013, Fibrous dysplasia in a 120,000+ year old Neandertal from Krapina, Croatia, *PloS One*, **8**(6), e64539.

Ong, T. M., Song, B., Qian, H. W., Wu, Z. L., and Whong, W. Z., 1998, Detection of genomic instability in lung cancer tissues by random amplified polymorphic DNA analysis, *Carcinogenesis*, **19**(1), 233–5.

Papagrigorakis, M. J., Karamesinis, K. G., Daliouris, K. P., Kousoulis, A. A., Synodinos, P. N., and Hatziantoniou, M. D., 2012, Paleopathological findings in radiographs of ancient and modern Greek skulls, *Skeletal Radiology*, **41**(12), 1605–11.

Rohland, N., and Hofreiter, M., 2007, Ancient DNA extraction from bones and teeth, *Nature Protocols*, **2**(7), 1756–62.

Schuenemann, V. J., Singh, P., Mendum, T. A., Krause-Kyora, B., Jager, G., Bos, K. I., Herbig, A., Economou, C., Benjak, A., Busso, P., Nebel, A., Boldsen, J. L., Kjellstrom, A., Wu, H., Stewart, G. R., Taylor, G. M., Bauer, P., Lee, O. Y., Wu, H. H., Minnikin, D. E., Besra, G. S., Tucker, K., Roffey, S., Sow, S. O., Cole, S. T., Nieselt, K., and Krause, J., 2013, Genome-wide comparison of medieval and modern *Mycobacterium leprae*, *Science*, **341**(6142), 179–83.

Schultz, M., 2001, Paleohistopathology of bone: a new approach to the study of ancient diseases, *American Journal of Physical Anthropology*, **Suppl. 33**, 106–47.

Sontakke, S. A., Karjodkar, F. R., and Umarji, H. R., 2011, Computed tomographic features of fibrous dysplasia of maxillofacial region, *Imaging Science in Dentistry*, **41**(1), 23–8.

Thompson, R. C., Allam, A. H., Lombardi, G. P., Wann, L. S., Sutherland, M. L., Sutherland, J. D., Soliman, M. A., Frohlich, B., Mininberg, D. T., Monge, J. M., Vallodolid, C. M., Cox, S. L., and Abd el-Maksoud, G., Badr, I., Miyamoto, M. I., el-Halim Nur el-Din, A., Narula, J., Finch, C. E., and Thomas, G. S., 2013, Atherosclerosis across 4000 years of human history: the Horus study of four ancient populations, *Lancet*, **381**(9873), 1211–22.

Toyosawa, S., Yuki, M., Kishino, M., Ogawa, Y., Ueda, T., Murakami, S., Konishi, E., Iida, S., Kogo, M., and Komori, T., 2007, Ossifying fibroma vs fibrous dysplasia of the jaw: molecular and immunological characterization, *Modern Pathology*, **20**(3), 389–96.

Unal Erzurumlu, Z., Celenk, P., Bulut, E., and Baris, Y. S., 2015, CT imaging of craniofacial fibrous dysplasia, *Case Reports in Dentistry*, **2015**, 134123.

Van Merkesteyn, J., Groot, R., Bras, J., and Bakker, D., 1988, Diffuse sclerosing osteomyelitis of the mandible: clinical radiographic and histologic findings in twenty-seven patients, *Journal of Oral and Maxillofacial Surgery*, **46**(10), 825–9.

Wade, A. D., Garvin, G. J., Hurnanen, J. H., Williams, L. L., Lawson, B., Nelson, A. J., and Tampieri, D., 2012, Scenes from the past: multidetector CT of Egyptian mummies of the Redpath Museum, *Radiographics*, **32**(4), 1235–50.

Wang, L. X., Ta, L., and Zhu, Y. G., 2010, *Linxi Jinggouzi: excavations and systematic research on cemetery of Late Bronze Age*, Science Press, Beijing.

Wells, C., 1963, Polystotic fibrous dysplasia in a seventh-century Anglo-Saxon, *British Journal of Radiology*, **36**, 925–6.

Willmon, R., Coqueugniot, H., Holowka, S., Dutour, O., and Pfeiffer, S., 2013, Fibrous dysplasia of the temporal bone: a case from the Glen Williams Ossuary, Ontario, Canada, *International Journal of Paleopathology*, **3**(4), 269–73.

Wu, X. J., and Schepartz, L. A., 2009, Application of computed tomography in paleoanthropological research, *Progress in Natural Science*, **19**(8), 913–21.